ICES
CIEM

International Council for
the Exploration of the Sea

Conseil International pour
l'Exploration de la Mer

Population projections of Pacific sardine driven by ocean warming and changing food availability in the California Current

Stefan Koenigstein [1,2,*], Michael G. Jacox[1,2,3], Mercedes Pozo Buil[1,2], Jerome Fiechter[4],
Barbara A. Muhling[1,5], Stephanie Brodie[1,2], Peter T. Kuriyama [5], Toby D. Auth[6], Elliott L. Hazen[1,2],
Steven J. Bograd[1,2] and Desiree Tommasi[1,5]

[1]Institute of Marine Science, University of California Santa Cruz, Santa Cruz, CA 95064, USA
[2]Environmental Research Division, NOAA Southwest Fisheries Science Center, Monterey, CA 92037, USA
[3]Physical Sciences Laboratory, NOAA Earth System Research Laboratories, Boulder, CO 80305, USA
[4]Ocean Sciences Department, University of California Santa Cruz, Santa Cruz, CA 95064, USA
[5]Fisheries Resources Division, NOAA Southwest Fisheries Science Center, La Jolla, CA 92037, USA
[6]Pacific States Marine Fisheries Commission, Newport, OR 97365, USA

* Corresponding author: tel: +1 (831) 502-8344; e-mail: stkoenig@ucsc.edu.

Small pelagic fish are important marine ecosystem components and highly variable fisheries resources. In the California Current upwelling system, Pacific sardine (*Sardinops sagax*) has supported important fisheries in the past, but contrary to expectations, remains at low biomass despite recent warm ocean conditions. We developed a data-driven, process-based population model that reproduces fluctuations of the US Pacific sardine population based on ocean temperature, early life stage and adult food, and upwelling strength. The lack of sardine recovery after 2014 can be explained by reduced food availability. Ensemble projections for the 21st century driven by downscaled ocean-biogeochemical simulations under three Earth system models (ESMs) show a likely recovery to early 2000s sardine abundance and catch by mid-century, due to increased recruitment. Ecological process uncertainty (ensemble configuration range) is of the same magnitude as uncertainty among ESM projections, and uncertainty related to the thermal optimum of early life stages dominates after 2070. Even for a fish species presumably favoured by warmer conditions, future climate projections entail risks of stock declines in food-limited years and when passing unknown thermal optima. Quantification of combined environmental driver impacts and sources of uncertainty to projections under novel conditions open new pathways for environment-responsive fisheries management strategies.

Keywords: climate change, environmental variability, forage fish, mechanistic model, population dynamics, small pelagic fish.

Introduction

Small pelagic fish (SPF) are an important component of marine ecosystems, and for direct fisheries and production of aquaculture feed (Pikitch *et al.*, 2014; FAO, 2020). The productivity of SPF such as sardine and anchovy is strongly driven by environmental drivers linked to climate, and their dynamics are characterized by pronounced cycles of collapse and recovery. The impacts of global climate change on SPF can therefore potentially be severe (Chavez *et al.*, 2003; Checkley *et al.*, 2017). However, incomplete understanding of the mechanisms behind SPF population fluctuations poses significant challenges for climate adaptation, fisheries management, and marine food security (Bakun, 2014; Essington *et al.*, 2015; Peck *et al.*, 2021).

The eastern boundary upwelling systems that are home to the largest SPF stocks are themselves highly variable physically and ecologically. Climate change is projected to lead to an increase in equatorward wind, and consequently, increased coastal upwelling on poleward ends of upwelling systems, with the opposite trend in equatorward portions (Rykaczewski *et al.*, 2015). However, the influence of changing winds on nutrient availability and biological productivity is complicated by changes in spatial patterns of upwelling,

stratification, and the nutrient content of upwelling source waters, and it is unclear how changes in primary productivity will be transferred to intermediate trophic levels, for example, SPF and top predators (Bakun *et al.*, 2015; García-Reyes *et al.*, 2015).

The California Current System (CCS) is an upwelling system where environmental variability is a primary driver of forage fish populations, which in turn impact the diet, condition, reproductive success, and mortality in different seabirds, California sea lions, humpback whales, and salmon (Checkley and Barth, 2009). In 2014–2016, a large marine heatwave (known as "The Blob," followed by a strong *El Niño* event) had drastic impacts on biological productivity in the CCS (Bond *et al.*, 2015; Cavole *et al.*, 2016; Jacox *et al.*, 2016), resulting in low forage availability and subsequent extreme mortality events for seabirds and California sea lions (McClatchie *et al.*, 2016; Piatt *et al.*, 2020).

Pacific sardine (*Sardinops sagax*, Clupeidae) has historically sustained the most important small pelagic fisheries in the CCS, and climate-driven fluctuations in abundance are recorded also on paleolithic timescales (McClatchie *et al.*, 2017). In the 1950s, sardine fisheries collapsed due to a combination of worsening environmental conditions and overfishing

(MacCall, 1979; Barnes *et al*., 1992). In the 1990s, the sardine population recovered temporarily, but started to decline again in the mid-2000s until the fishery was closed in 2015 (PFMC, 2017). Statistical analyses have related sea surface temperature (SST) or the Pacific decadal oscillation (PDO) to sardine recruitment and biomass (Jacobson and MacCall, 1995; Lindegren and Checkley, 2013; Zwolinski and Demer, 2014). However, the positive correlation of ocean temperature with sardine recruitment is dependent on system state (Sugihara *et al*., 2012; Deyle *et al*., 2013). The recent sardine collapse during a period of elevated SST has put the linear SST–recruitment relationship into question (McClatchie *et al*., 2010; Zwolinski and Demer, 2019), and statistical habitat models trained on pre-heatwave data failed to reproduce the spatial distribution shifts in Pacific sardine to warmer waters after 2014 (Muhling *et al*., 2020).

As statistical correlations with SST and large-scale climate indices have proven insufficient to explain sardine dynamics, and novel environmental conditions linked to climate change are emerging in the CCS, there is a need to advance the incorporation of biological mechanisms to increase understanding of how the environment shapes dynamics of SPF populations. Multiple environmental drivers affect the response of fish populations to climate change through impacts on recruitment, reproduction, survival, growth, and behaviour (Rijnsdorp *et al*., 2009; Pörtner and Peck, 2010; Koenigstein *et al*., 2016). Specifically, climate impacts on SPF populations are mediated by temperature-dependent vital rates, especially in early life stages (ELS), planktonic food availability, adult condition and habitat availability, predation pressure, and oceanographic mechanisms, such as offshore transport (Takasuka *et al*., 2007; Peck *et al*., 2013; Nieto *et al*., 2014; Checkley *et al*., 2017). Considering all of these factors in an integrative modelling framework is needed to understand the relative contributions of drivers of SPF dynamics.

Highly dynamic SPF–upwelling systems can serve as model systems to improve understanding of environmental variability on marine fish population dynamics, and the responses of climate–ocean–fisheries systems to global change (Bakun, 2014; Peck *et al*., 2021). High-resolution ocean-biogeochemical (BGC) models are powerful tools to investigate future changes in regional oceans, providing detailed projections of changes in upwelling, ocean warming, deoxygenation, acidification, and lower trophic level productivity in the CCS in the course of the 21st century (Xiu *et al*., 2018; Fiechter *et al*., 2020; Pozo Buil *et al*., 2021). While some ecosystem models build upon ocean models and include physiological processes for SPF (e.g. Kaplan *et al*., 2018; Politikos *et al*., 2018), it is challenging to assess uncertainty of these complex models for application in fisheries managment and climate change adaptation (Kaplan *et al*., 2018; Drenkard *et al*., 2021).

We developed a mechanistic, age-structured population model of intermediate complexity for ecosystem assessment (Plaganyi *et al*., 2012; Punt *et al*., 2016) for the northern subpopulation of Pacific sardine in the CCS. The model provides a full life cycle, process-based integration of environmental drivers, and integrates available survey data, stock assessment model output, and high-resolution regional ocean model projections. An ensemble model configuration set spanning a wide range of possible parameter combinations that reproduce the recent boom and bust of the sardine population is used to bracket ecological uncertainty. Population abundance and spatial distribution are projected under downscaled ocean-BGC model projections until 2100, identifying mechanisms driving population-level responses and trends. Additional uncertainty to long-term population trajectories related to the response to novel temperature regimes is quantified by sensitivity analysis. This work improves the potential for understanding of SPF population drivers, quantification of uncertainty, and mid- and long-term prediction under novel environmental conditions due to climate change.

Material and methods

Adult population model

The model is an age-structured dynamic population model for Pacific sardine (cf. Butler 1993).. We used the system dynamics modelling software STELLA Architect V.2.15, which constructs finite difference equation systems from a graphical "stocks and flows" annotation (www.iseesystems.com). Arrayed "conveyor" stock elements contain yearly cohorts with monthly substocks of (a) nonfeeding ELS (eggs and nonfeeding larvae), (b) feeding larvae and juveniles (cf. the "ELS survival, adult consumption, and egg production" section), and (c) adult sardine individuals (Figure 1a). Monthly, the content of each substock i becomes the inflow of the next substock $i+1$. Different mortality rates (see below) are subtracted as linear "leakage flows" of the conveyors. Model equations (Table 1) were solved for a dt of 1/16 month using Runge–Kutta fourth-order integration.

Adult stocks are calculated for individuals of each age class 1–8 with age-dependent fishing, predation, and background (natural) mortalities [Table 1, Equation (1.1)]. Fishing mortality rates per age class n for each of two fleets f [Mexican–Californian (*MexCal*) and Pacific Northwest (*PNW*)] are based on fleet age selectivity, geographical access, and sardine latitudinal position [Table 1, Equation (1.2)]. Predation mortality is caused by a generic predator stock, representing all predators that respond to sardine density, such as California sea lions and brown pelicans [Table 1, Equation (1.3); Punt *et al*., 2016; Kaplan *et al*., 2018].

ELS survival, adult consumption, and egg production

To determine recruitment to the adult population, the model uses dynamically calculated eggs and pre-feeding larvae [Table 1, Equation (2.1)] with temperature-dependent mortality and development time, food-dependent late larvae and juvenile starvation mortality [Table 1, Equation (3.1)], and a time-varying calculation of consumption- and age-dependent egg production. While static relationships of spawner biomass to recruitment are traditionally used in fisheries stock assessment models, they do not successfully describe recruitment variation in SPF stocks (Canales *et al*., 2020). Eggs and pre-feeding larvae have a temperature-dependent ELS mortality to integrate the established physiological effects of temperature on survival rate [Table 1, Equation (2.2)] and stage duration [Table 1, Equation (2.3)], resulting in thermal performance curves for survival, which can be experimentally quantified (Pörtner and Peck, 2010; Koenigstein *et al*., 2018). Thermal optima for ELS survival outside of the model calibration temperature range are varied in sensitivity analysis during projections (cf. the "Model ensemble configurations and projections" section). The effective temperature for eggs and
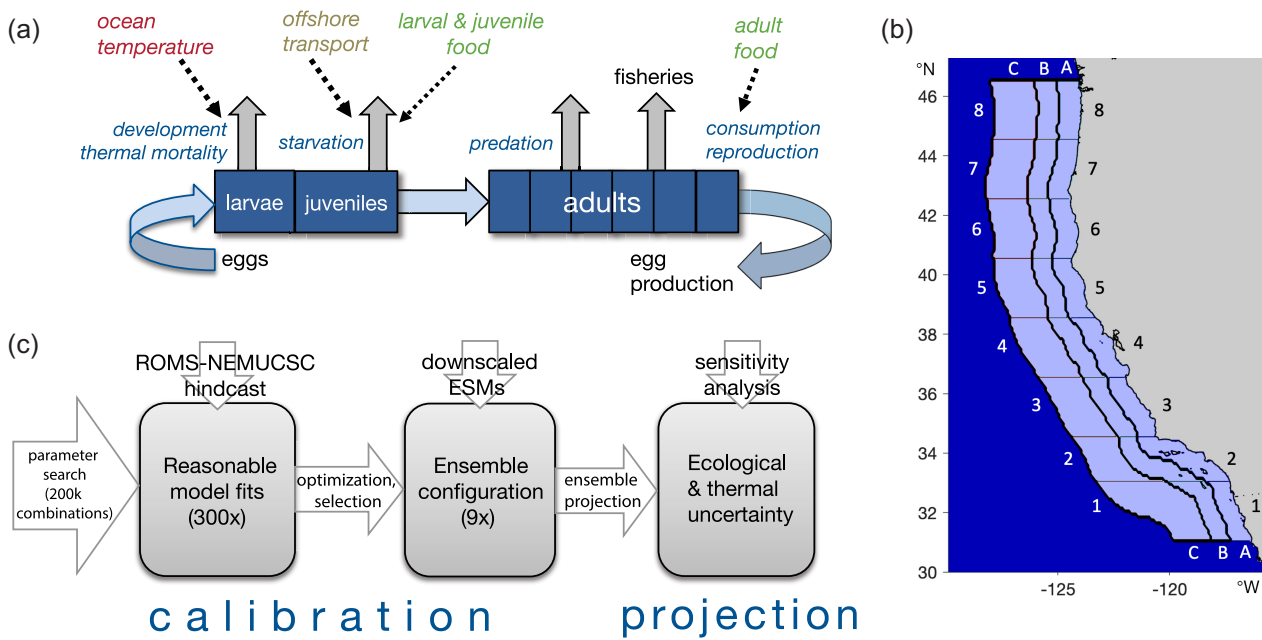
Figure 1. (a) Structure of the sardine population model with incorporated biological processes and environmental drivers; (b) model domain with 24 spatial zones for integration of ROMS-NEMUCSC output and observation data; and (c) workflow for model calibration, ensemble configuration, and projections

pre-feeding larvae T_e is calculated by weighting SST input data according to ELS distribution among zones of the model domain, and feeding larvae and juveniles [Table 1, Equation (3.1)] have a starvation mortality rate dependent on current larval-juvenile food [nanophytoplankton and microzooplankton; Equation (3.2)] within the ELS distribution (cf. the "Spatial distribution" section).

Adult individual consumption per food item [Table 1, Equation (4.1a, b)] is based on three different food items (diatoms, mesozooplankton, and krill), weighted by the current adult sardine distribution in the model domain, and constrained by a "soft" population carrying capacity per model cell, above which individual consumption linearly decreases [Equation (4.2a, b)]. Sardine total egg production depends on total consumption, and reproductive investment increasing with age class depending on model configuration [Table 1, Equation (4.3)].

Spatial distribution

Annual spatial distribution is simulated for sardine ELS (eggs, larvae, and juveniles) and feeding adults to approximate the effects of the annual sardine migration on ELS survival and adult egg production (Demer *et al.*, 2012) by calculating distribution-integrated means of SST and planktonic food availability. Fractions of ELS and adults are arrayed across the 24 model zones (Figure 1b) based on SST and upwelling strength (for ELS) and food biomass (for adults) as described below.

ELS distribution is fitted to egg and larvae data for the northern subpopulation of Pacific sardine in spring (April–June) during 2003–2018 (Supplementary Figure S2) from the California Cooperative Oceanic Fisheries Investigations (CalCOFI) programme and additional surveys in the northern CCS (Auth *et al.*, 2018; NOAA SWFSC, 2022). The latitudinal centre of gravity (COG) of ELS distribution is determined for

each model year by the row of cells with an SST closest to an optimum spawning temperature T_{SPA} calculated during model calibration. The fractions of ELS (c_s) in remaining model zones decay quadratically [Table 1, Equation (5.1)].

ELS distribution on the longitudinal (distance to coast) axis is adjusted dynamically to simulate larval offshore transport, by linear regression of the annual historical longitudinal COG from the CalCOFI data to the CUTI (Coastal Upwelling Transport Index) upwelling index for the core upwelling region in model zones 4–7 (Supplementary Figures S2 and S6; Jacox *et al.*, 2018). The final egg and larvae fractions are used to weigh the SST and plankton group input data from the 24 spatial zones to calculate the annual ELS temperature T_e and larval-juvenile food availability $D_{1,2}$ (see above).

Adult feeding distribution is calculated by determining an annual feeding latitudinal COG based on the latitude of highest biomass density of the primary food item among spatial cells, and sardine migration distance as the distance from the spawning latitudinal COG for the same year, multiplied by a forage migration factor FM resulting from model calibration. The decaying fraction of feeding adults (c_a) in remaining spatial cells depends on model configuration [Table 1, Equation (5.2)]. Adult distribution on the longitudinal (distance to coast) axis is kept constant at the annual mean adult distribution among zones from acoustic-trawl surveys (Zwolinski *et al.*, 2012; 50% of adults in zone B, 25% in zones A and C). The final distribution of feeding adults is used to weigh available adult food biomass D_f (see above) to calculate food availability averaged over the adult distribution.

Ocean-BGC model forcing and future projections

Environmental drivers for model calibration and projection were output from a high-resolution CCS configuration of the Regional Ocean Modeling System (ROMS) coupled with the NEMUCSC BGC model (Fiechter *et al.*, 2020), a version of

Table 1. Model equations and parameters.

Equation number	Category (parameter)	Equation (description)
1.1	**Adult population**	$A_{n,\,i\,(t)} = A_{n,\,i\,(t-dt)} + (I_{n,\,i\,(t)} - I_{n,\,i\,0}\,(F_{n\,(t)} + p * P_{(t)} + M_n)) * dt$
	$A_{n,i(t)}$ $A_{n,i(t-dt)}$	Number of adults of a monthly cohort in substock i of age class n at time t, and at the previous time step
	$I_{n,i(t)}$	Inflow of new individuals from the previous substock (= outflow of the previous age class for the first substock; outflow of the last juvenile substock for the first age 1 substock inflow)
	$I_{n,i0}$	Original inflow into the first substock i time steps prior ($= I_{n,1\,(t-i*dt)}$)
	$F_{n(t)}$	Sum of age-dependent adult fishing mortality rates from two fleets [Equation (1.2)]
	$p * P_{(t)}$	Predation mortality rate due to a dynamically responding predator stock (see below)
	M_n	Age-dependent background (natural) mortality rate
1.2	**Fisheries mortality**	$F_{n,\,f\,(t)} = \frac{C_{n,f(t)}}{N_{n(t)}} * s_{n,f} * a_f * L_{(t)}$
	$C_{n,f(t)}$	Catch (number of individuals) per age class and fleet
	$N_{n(t)}$	Total sardine number per age class
	$s_{n,f}$	Fisheries selectivity at age class
	a_f	Geographical fleet availability factor
	$L_{(t)}$	Annual latitudinal position of sardine habitat within the model domain (midpoint between spawning and feeding habitat COG, scaled between 0 and 1; cf. "*spatial migration*")
1.3	**Predation**	$P_{(t)} = P_{(t-dt)} + ((g_p + p * A_{tot\,(t)} * f_p)_{(t)} - P_{(t-dt)}{}^2 * m_p) * dt$
	$L_{(t)}$	Predator number at time t
	g_p	Base predator growth rate in the absence of sardine
	$p * A_{tot(t)}$	Consumption of sardine adults by the predator
	f_p	Predator feedback rate (i.e. efficiency of utilization of sardine consumption)
	m_p	Quadratic predator natural mortality rate
2.1	**Nonfeeding ELS**	$E_{i(t)} = E_{i\,(t-dt)} + (H_{i\,(t)} - H_0\,M_e) * dt$
	$E_{i(t)}$	Number of developing eggs or early larvae in substock i at time t
	H_0	Number of newly hatched eggs
	$H_{i(t)}$	The inflow from the previous substock (= H_0 for the first substock)
	M_e	Temperature-dependent ELS mortality rate
2.2		$M_e = 1 - M_t{}^{(t_d)}$
	M_t	Thermal mortality per development time step
2.3		$M_t = (1 - T_b) * (1 - e^{-T_s * (T_{lim} - T_e)})$
	T_b	ELS background (natural) mortality rate
	T_s	Slope of thermal mortality
	T_{lim}	Maximum survival temperature (physiological thermal limit)
2.4	**Development time**	$t_d = d_{temp} * e^{-d_s * T_e} + d_{min}$
	d_{temp}	Duration of the temperature-sensitive period of ELS development
	d_s	Development time slope
	d_{min}	Minimum development time (months)
	T_e	Mean temperature experienced by ELS (°C)
3.1	**Feeding ELS**	$J_{i\,(t)} = J_{i\,(t-dt)} + (K_{i\,(t)} - J_0\,(M_j + S)) * dt$
	$J_i(t)$	Number of developing eggs or early larvae in position i of the substock at time t
	J_0	Number of new feeding larvae (final substock of E_i)
	$K_{i(t)}$	The inflow from the previous substock (= J_0 for the first substock)
	M_j	Late larval-juvenile background mortality rate
	S	Starvation mortality rate
3.2	**Starvation**	$S = (s_1\,D_1 + s_2\,D_2)$
	$s_{1,2}$	Starvation rates for diet items 1 (nanophytoplankton) and 2 (microzooplankton)
	$D_{1,2}$	Relative fractions of historical maximum biomass for diet items 1 and 2, weighted over sardine feeding larvae and juvenile spatial distribution in the model domain
4.1a, b	**Consumption**	$Q_{f\,(t)} = D_{f\,(t)} * (1 - Q_{f\,\min}) + Q_{f\,\min}$ if $N_{tot\,(t)} < K'_{(t)}$
		$Q_{f\,(t)} = Q_{f\,\max} * \frac{K'}{N_{tot}}$ if $N_{tot\,(t)} \geq K'_{(t)}$
	$D_{f(t)}$	Current biomass at time t of adult food item f (for diatoms, mesozooplankton and krill; weighted by the current adult sardine distribution in the model domain, see the "Ocean-BGC model forcing and future projections" section)

Table 1. Continued

Equation number	Category (parameter)	Equation (description)
	Q_{fmin}	Consumption at minimum biomass level for food item f
	Q_{fmax}	Maximum consumption of food item f
	$N_{tot(t)}$	Current total adult population number ($= \Sigma A_{n,i(t)}$)
	K'	Distribution-integrated, "soft" population carrying capacity
4.2a, b	**Local carrying capacity**	$K'_{(t)} = LD * \sum N_{k\,s\,(t)}$ if $LD * \sum N_{k\,s\,(t)} > K_{min}$
		$K'_{(t)} = K_{min}$ if $LD * \sum N_{k\,s\,(t)} \leq K_{min}$
	$N_{ks(t)}$	Number of sardine above the carrying capacity for each of the 24 model zones at time t (i.e. $N_{s\,(t)} - K'/24 > 0$, where $N_{s\,(t)}$ is current number of sardine per zone)
	K_{min}	Minimum total carrying capacity below, which there are no density-dependent effects
	LD	Local density dependence factor in the range between 0 and 1
4.3	**Reproduction**	$R_{tot} = \sum (\sum Q_f * N_n * RI_n)$
	ΣQ_f	Total individual consumption of the three adult food items
	N_n	Number of individuals per age class
	RI_n	Annual reproductive investment, as fraction of consumed food biomass per age class
5.1	**ELS distribution**	$c_s = \frac{1}{\Delta_{s\,lat}^2}$
	Δ_{slat}	Distance in model zones to the ELS COG on the latitudinal axis
5.2	**Adult distribution**	$c_a = \frac{1}{\Delta_{f\,lat}^{CF}}$
	Δ_{flat}	Distance to the feeding COG on the latitudinal axis in model domain cells
	CF	Adult concentration factor (range 0.5–3)

See Supplementary section S1 for further information on model calibration, and Supplementary Table S1 for ensemble configuration parameter values.

North Pacific Ecosystem Model for Understanding Regional Oceanography (NEMURO, Kishi *et al.*, 2007) specifically parameterized for the CCS. The ROMS-NEMUCSC output provides (a) SST and the CUTI upwelling index to inform sardine spawning habitat, ELS offshore transport and temperature-dependent ELS mortality, and (b) biomass of two phytoplankton and three zooplankton groups to determine feeding habitat, feeding larvae, and juvenile survival, and adult consumption and egg production (cf. the "ELS survival, adult consumption, and egg production" and "Spatial distribution" sections).

For model calibration (cf. the "Model ensemble configurations and projections" section, Supplementary section S1), output from a ROMS-NEMUCSC hindcast for 1980–2010 was used (Pozo Buil *et al.*, 2021). The ability of the model to capture the 2011–18 decline in sardine abundance under relatively warm SST was tested by forcing with additional SST output from a near-real time data assimilative version of the CCS ROMS model (Neveu *et al.*, 2016; oceanmodeling.ucsc.edu) and fisheries landings data (no fishing after 2014 due to low estimated biomass). As high-resolution plankton output was not available from ROMS-NEMUCSC for 2011–18, we used food availability at the historical low of total plankton biomass from the 1980–2010 ROMS-NEMUCSC hindcast and tested sensitivity of the configurations by comparing to simulations using the historically highest value (Supplementary Figure S1).

For future projections, three Earth system models (ESMs) from the Coupled Model Intercomparison Project 5 (CMIP5) were regionally downscaled using ROMS-NEMUCSC with the time-varying delta method under Representative Concentration Pathway (RCP) 8.5 (a high emissions scenario). The three models, the Geophysical Fluid Dynamics Laboratory ESM2M (termed GFDL hereafter), the Institut Pierre Simon Laplace CM5A-MR (IPSL), and the Hadley Centre

HadGEM2-ES (HAD) were chosen to capture the CMIP5 range of projected future changes in physical and BGC CCS properties (Pozo Buil *et al.*, 2021).

Model ensemble configurations and projections

We identified an ensemble of nine different model configurations, which span the ranges of parameter values and projected total sardine abundances for a wide range of possible model configurations with good historical fits (Supplementary Material). Identical among all ensemble configurations, annual spawning location was fitted to CalCOFI egg and larval survey data (cf. the "Spatial distribution" section), and fisheries mortality rates per age class were fit to total annual landings and age composition for two fleets from a Pacific sardine stock assessment model spanning the sardine population boom-bust cycle during 1980–2019 (Supplementary Table S2, Supplementary Figures S2 and S5). All other model parameters were estimated by fitting to numbers at age 1980–2010 from the same stock assessment model, identifying alternative configurations by a wide parameter search in a multi-step process using sensitivity analyses and parameter optimization (Figure 1c).

During projections, ELS COG follows T_{SPA} obtained from fitting to data and is therefore the same across ecological ensemble members. By contrast, feeding adult COG is determined by the zone of highest availability of the primary adult food item, and a maximum migration distance specific to each ensemble configuration (cf. the "Spatial distribution" section). Total annual catch $C_{tot} = \sum C_{n,f}$ for future projections is set at a constant fraction of population abundance in the previous year, found by linear regression of 1980–2014 data, using a catch cut-off value at 150.000 tons, approximating the current harvest guideline (Supplementary section S1).

To assess the impact of future novel temperature regimes outside of the model calibration range ("thermal uncertainty"), the parameter for the critical thermal limit T_{lim} (which also determines the emerging optimum temperature for larval survival T_{opt}) was varied within the range of projection temperatures in an additional sensitivity analysis. T_{lim} was varied in 0.5°C steps between the lowest T_{lim} with an impact on the fit during the calibration period (>99% of best R^2 for total abundance) and the highest T_{lim} with a significant impact on projections (>1% deviation in any annual abundance value) to bracket the thermal uncertainty range (Supplementary Figure S8).

Results

Model fit during calibration period

The model ensemble configuration includes nine distinct parameter combination sets fitted to reproduce sardine numbers-at-age estimates for 1980–2010. Each provides a good fit to the stock assessment estimate of total annual adult sardine abundance ($R^2 = 0.62$–0.83) during the combined fitting and testing period 1980–2018, while the best alternative model configurations using only temperature or part of the food-dependent processes explain less of the variance in historical abundance (Supplementary Material).

Between 2004 and 2010, an adult density-dependent reduction in egg production paired with subaverage recruitment success during several cooler years led to a decline of the sardine stock (Figure 2). During 2011–18, the collapsed sardine population, despite warmer SST and low or no fishing, is reproduced by the model under low food availability due to increased ELS starvation and additional impacts of low egg production in some configurations (Supplementary Figures S3 and S4). Under a high food availability scenario, the stock would have recovered to different degrees depending on model configuration (Supplementary Figure S1).

Temperature-related ELS mortality is a major driver of recruitment success in all ensemble configurations, and none of the configurations suggests that temperatures during the calibration period 1980–2010 have already exceeded the optimal range for ELS. T_{opt} ranges from 14.8°C to above 17.7°C (the highest temperature reached in the sardine spawning habitat during projections) according to the fitted shape and T_{lim} of the ELS temperature response (Supplementary Figure S7).

Fitting to spatial egg and larval data resulted in an ideal spawning habitat SST at $T_{SPA} = 13.5$°C, consistent with results of spatial habitat models for the northern subpopulation of Pacific sardine in the CCS (Weber and McClatchie, 2010; Zwolinski *et al.*, 2011; Muhling *et al.*, 2020), and the northward shift in spawning habitat observed during 2015–16 is approximated (Supplementary Figure S2).

Ensemble sardine abundance projections

Recovery and generally increasing trends in sardine abundance over the course of the 21st century emerge in the ensemble mean under all downscaled projections (Figure 2). A likely return to abundance levels of the early 2000s (15–28 billion adult sardine) is projected by mid-century due to increasing recruitment success under warming SST (Figure 2). One extreme model configuration shows sardine abundance remaining continuously low until late in the projections, but

this configuration was deemed biologically unlikely (Supplementary section S1).

Decadal-scale fluctuations in periods of 15–30 years with high sardine abundance for durations of 2–8 years are produced to different extents among model configurations (Figure 2). The highest abundance peaks in the ensemble (100 billion sardine individuals in the HAD and IPSL projections under two model configurations from the ensemble), are largely consistent in timing with fluctuations to abundance peaks of 30–60 billion individuals in some of the other model configurations.

After 2060, in HAD and IPSL projections, which include significantly higher warming rates than GFDL, ensemble means for most years show sardine abundance above peak numbers seen in the early 2000s (25–34 billion), while abundance under GFDL remains under 20 billion until the final years of the projection. Abundance increases are primarily linked to lowered ELS thermal mortality, leading to mean recruitment success at up to three to six times the level of the historical period in the second half of the HAD and ISPL projections. By contrast, in the GFDL projection, ELS survival generally fluctuates around the level of the calibration period with higher ELS survival in a warm period in 2040–45, and a slightly increasing trend after 2070.

Ensemble mean egg production per individual shows a marked decrease after 2045 under HAD and IPSL projections, with egg number per sardine fluctuating around 25–50% of the calibration period mean (Figure 2, centre panel). Under GFDL, a more moderately decreasing trend is recorded after 2075. Decreases in egg production per individual are linked to density-dependent reductions in adult consumption, and decreases in adult food biomass (diatoms, mesozooplankton, and krill) especially under HAD.

In contrast to the HAD and IPSL projections, increases in sardine abundance and catch are more limited by higher rates of ELS starvation in the GFDL projection, due to lower total nanophytoplankton and microzooplankton biomasses and exacerbated by offshore transport. The lower rate of surface water warming in the GFDL projection limits compensation of ELS starvation rates by decreases in ELS thermal mortality until late in the projection, with the exception of three consecutive warm years leading to a good sardine stock in mid-century. Model sensitivity tests with food-dependent processes disabled further illustrate that sardine increases under the projected warming regimes will be limited by variability and trends in food availability (Supplementary Material).

During 2061–82 in the IPSL projection, sardine abundance is very stable. This is caused by reduced variability in SST, nanophytoplankton, copepods, and krill during a period of weakening upwelling-favourable winds, linked to a positive phase of the PDO index in the underlying IPSL original solution (Pozo Buil *et al.*, 2021: Supplementary Material).

Uncertainty related to ELS thermal limits quantified by sensitivity analysis increases after 2060, as temperatures move beyond the range of the model calibration period, with impacts on sardine abundance starting between 2030 and 2080, depending on model configuration and ESM (Supplementary Figure S8). Across ecological and thermal uncertainty ranges, high sardine abundance (>40 billion) is more likely later in the HAD and IPSL projections; however, stock collapses to below cut-off limits for sardine fisheries also occur more often after 2080 (Figure 3). Under GFDL, the risk for fisheries closures is highest during 2060–80.
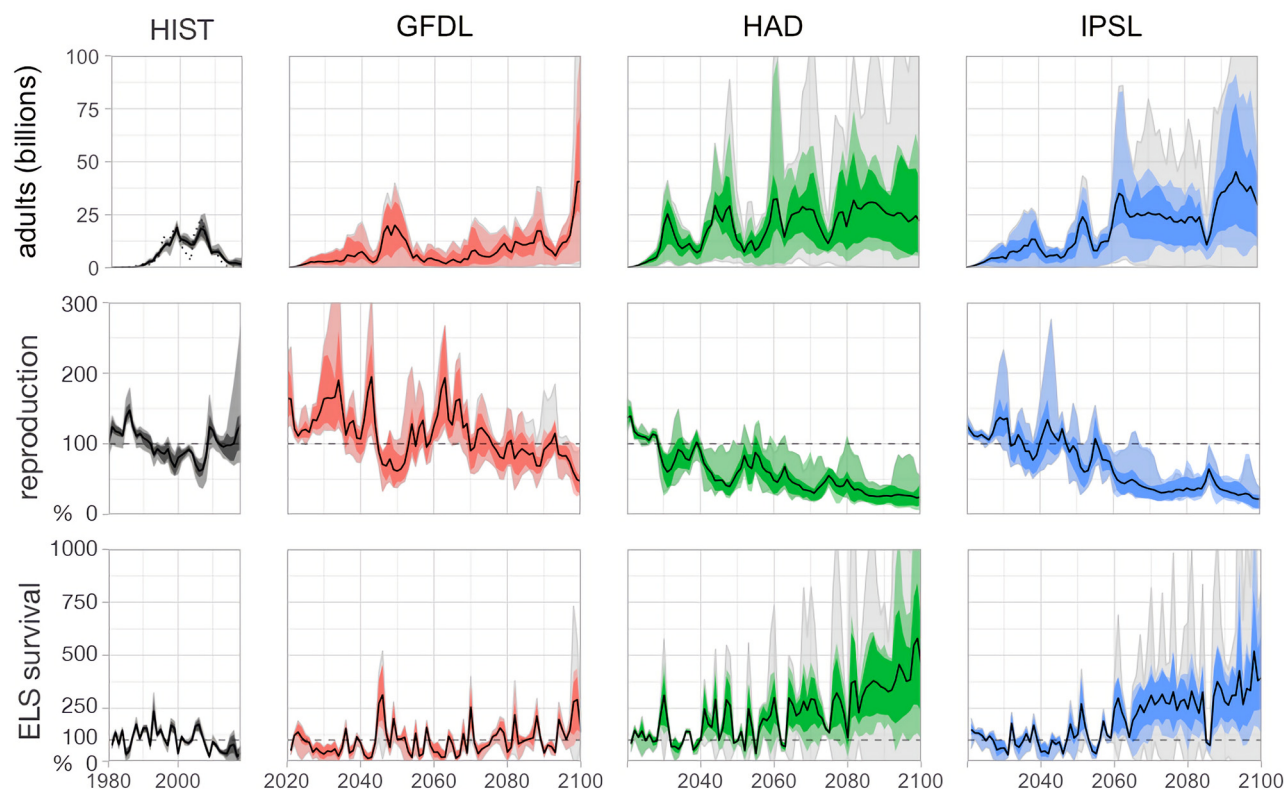
Figure 2. Sardine adult abundance (top), reproduction (relative egg production per adult; centre row), and ELS survival (relative recruits per egg; bottom). Mean and range of model ensemble configurations, during model calibration ("HIST"; dotted line: stock assessment abundance estimate) and in future projections under three different downscaled ESMs (GFDL, HAD, IPSL; lighter coloured fill: full ensemble range for means of thermal sensitivity of nine model configurations, darker coloured fill: range for seven configuration means without highest and lowest). Grey shaded area: thermal window uncertainty range, from sensitivity analysis of thermal optima for ELS in all configurations. Reproduction and ELS survival are shown as relative to mean during calibration period (dashed horizontal line).
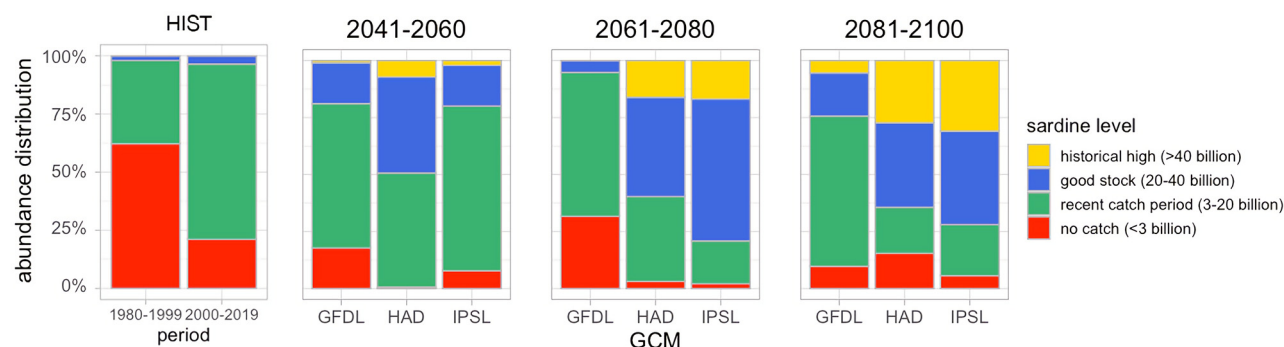
Figure 3. Distribution of sardine abundance across 20 years periods, during model calibration (HIST) and under projections of three downscaled ESMs (GFDL, HAD, and IPSL), including ecological uncertainty (nine ensemble model configurations) and thermal uncertainty (ELS temperature sensitivity ranges). Sardine abundance is separated into four categories (bottom to top): 1. "No catch": sardine below the harvest cutoff (<3 billion sardine); 2. "recent catch period": sardine harvested at up to 1990s–2000s peak abundance (3–20 billion); 3. "good stock": sardine above to twice of 1990s–2000s peak levels (20–40 billion); and 4. "historical high" sardine at or above 1930s abundance (>40 billion).

Projected sardine landings, spawning, and feeding locations

Projected sardine landings are a proportional, but smoothed, reflection of sardine abundance, except for years when the stock is under the harvest cut-off value and the fishery is closed (Figure 4). Landings show a recovery to catch levels of the early 2000s in ensemble means at 1.5–2.5 billion sardine around 2050. In the GFDL projection, landings decrease after that and recover to mean levels around 1–1.5 billion after 2070. Under HAD and IPSL, landings increase beyond 2.5

billion sardine in the ensemble mean after 2060, with extreme configurations reaching catch levels of 7–8 billion sardine during abundance peaks (based on the historical stock-catch relation, not considering potential socio-economic limitations in fleet or production capacity). Sensitivity of the modelled sardine population to changing fisheries mortality rates differs slightly among model configurations for the calibration period (Supplementary Figure S9).

Following the mean annual sardine latitudinal position, there is considerable interannual variability in relative
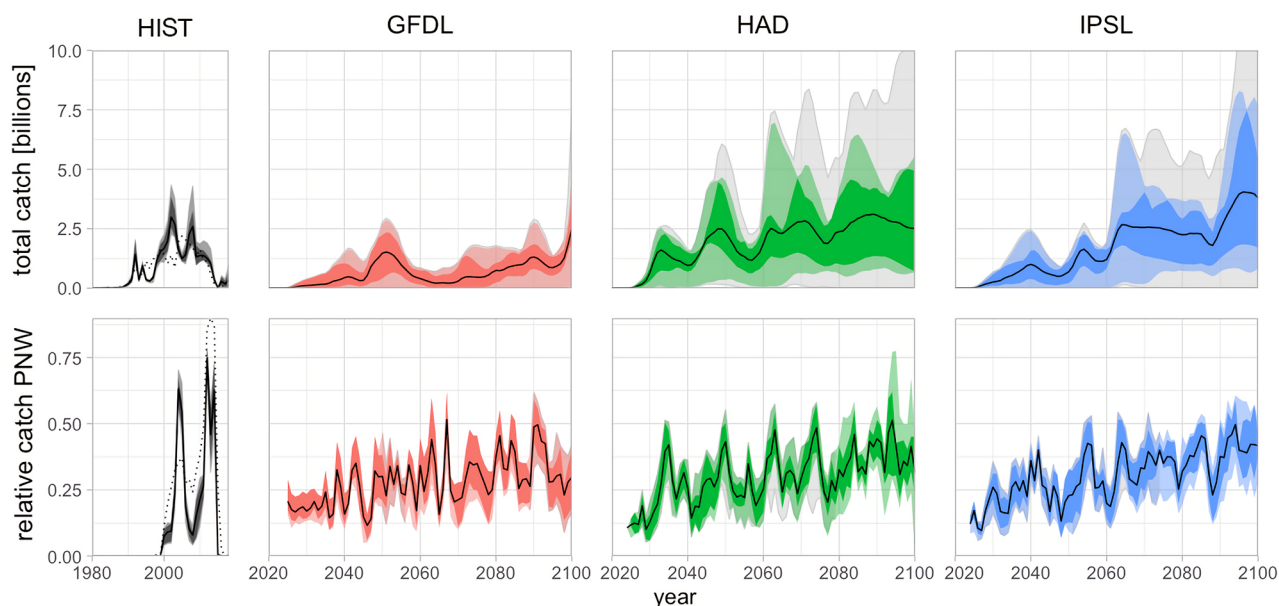
Figure 4. Total projected sardine catch (top) and relative contribution of the PNW fleet (bottom). Mean and range of model ensemble configurations during model calibration ("HIST"; dotted line: total landings estimates from stock assessment), and in future projections under three different downscaled ESMs (red: GFDL, green: HAD, and blue: IPSL; lighter fill: full range of nine configurations, darker fill: range for seven configurations without highest and lowest). Grey shaded area gives thermal window uncertainty range from sensitivity analysis of thermal limits for ELS for all configurations. Based on fitted fleet selectivity per age class, future total catch assumes a constant harvest control rule based on historical landings and stock data (cf. the "Adult population model" and "Model ensemble configurations and projections" sections).

composition among the two fishing fleets. In the long-term, the northward shift in habitat leads to increased availability and a relative increase in catches for the PNW fishing fleet, which reaches 30–50% of the total catch (combined PNW, Californian, and Mexican fleets) at the end of the century. While age composition of the catch fluctuates interannually, it remains constant on a long-term basis (Supplementary Figure S5).

Sardine spawning habitat progressively moves northward in future projections. Under GFDL, which projects a slower rate of warming than the other two ESMs, spawning habitat shows increased latitudinal variation during 2041–2080 and moves northward slower than under HAD and IPSL. Spawning occurs mainly in the northern half of the CCS after 2040 (HAD and IPSL) or 2060 (GFDL), and is compressed in the northernmost part of the domain by 2080–2100 (Figure 5, bottom). Adult feeding habitat, which follows highest food availability, moves north at a slower rate, reaching an interannual mean location at 39.5°N after around 2060 with variation among model configurations after 2080, driven by the main food item used as a cue for migration (Figure 5, top).

Cross-shore distribution of ELS varies interannually, influenced by offshore transport linked to upwelling strength (CUTI) with no discernible trend over projections. Reduced ELS food availability by offshore transport causes additional ELS starvation mortality and a reduction in recruitment success, more pronounced in the first half of the projections.

Discussion

Environmental mechanisms driving sardine populations

The nine mechanistic, age structured model configurations in our ensemble reproduce the sardine stock boom and bust during the model calibration and testing period 1980–2018. Considering planktonic food availability, upwelling strength, and

spatio-temporal variability in sardine spawning and feeding habitats in the CCS, a generally positive correlation of recruitment success with SST in the spawning habitat is identified as a primary driver of sardine population variability, in agreement with the results from other statistical and population modelling approaches (Jacobson and MacCall, 1995; Lindegren and Checkley, 2013).

Temperature-dependent variability in recruitment success is, however, modulated by changing food availability for ELS to different degrees among model configurations. The highest ELS starvation rates in the calibration period are reached in 1983–84 and 1997 under low nanophytoplankton and microzooplankton levels in ROMS-NEMUCSC. These years coincide with periods of low upwelling-favourable winds and two strong *El Niño* events, which led to low phytoplankton and zooplankton biomasses in the main sardine spawning areas in Southern California (Lavaniegos and Ohman, 2007; Venrick, 2012). Adult consumption and egg production contribute further variability, agreeing with the linkage between parental prespawning condition and Pacific sardine recruitment strength (Zwolinski and Demer, 2014). An individual-based model for CCS sardine coupled to a comparable ocean-BGC model also finds recruitment variations during 1986–2006 being shaped by variations in both egg production and ELS survival, with only moderate decreases in food availability for sardine larvae caused by offshore transport (Politikos *et al.*, 2018).

Our results point to low food availability for ELS as inhibiting the recovery of sardine during the model test period of 2011–18, with reduced egg production under lower adult food availability contributing to the decline in some model configurations. Due to the lack of a ROMS-NEMUCSC hindcast after 2010, we are assuming food availability at historical low levels in our model during that period. This is supported by empirical data indicating low planktonic food
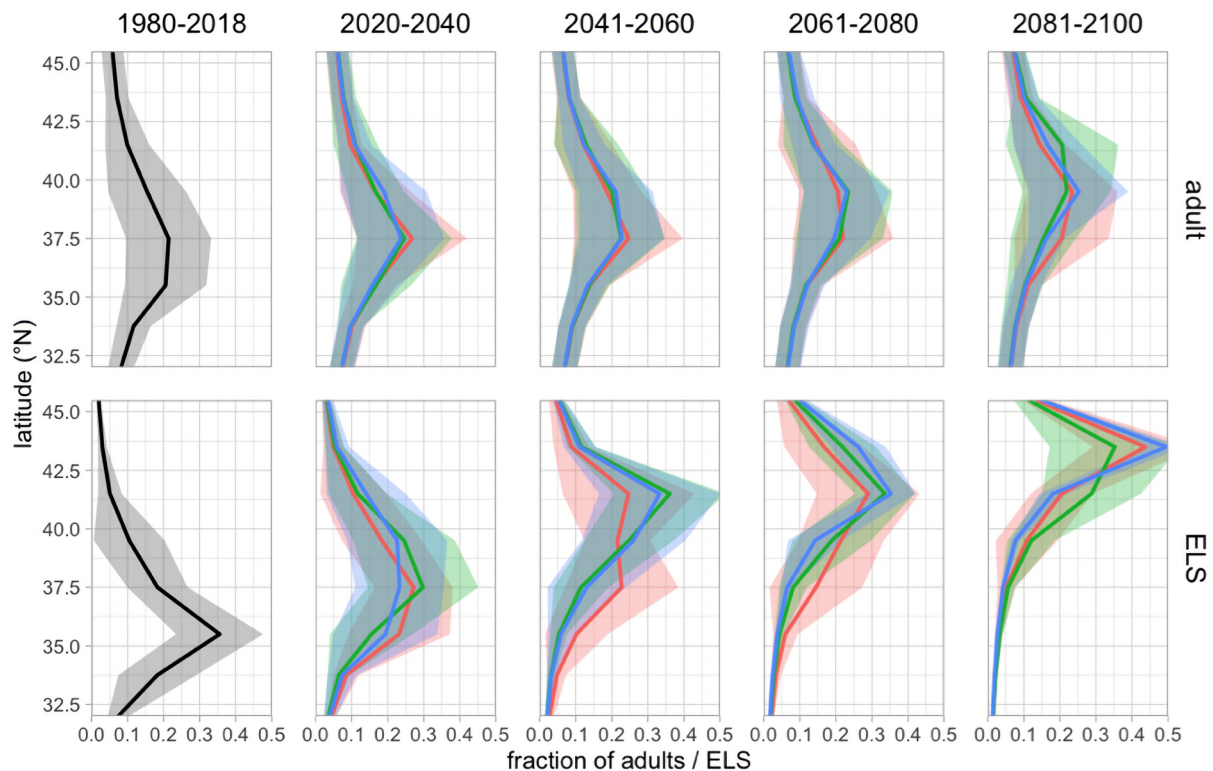
Figure 5. Latitudinal distribution of projected spawning and feeding habitat during model calibration (left column), and by 20 years time period under projections of three downscaled ESMs (red: GFDL, blue: HAD, and green: IPSL). Means (lines) and *SDs* (coloured areas) among ensemble model configurations by latitudinal model cell for fractions of feeding adults (top, based on different food migration cues and maximum migration distances from spawning habitat), and ELS (bottom, fitted to data and constant among model configurations).

availability for forage fish in the CCS during those years (Gómez-Ocampo *et al.*, 2018; Brodeur *et al.*, 2019). Tested with high food availability, most configurations show a return to early 2000s stock abundance by 2018, demonstrating that within our model, low food availability is a necessary prerequisite to explain the lack of recovery of the sardine stock during the last decade. Further analyses of how both oceanographic and ecological drivers (e.g. via competition) have affected sardine food availability during recent years could corroborate these findings.

Sardine abundance and landings projections exhibit periodic decadal-scale fluctuations (boom-and-bust cycles) on timescales of 15–30 years, similar to the oscillations recorded in historical SPF landings data and stock estimates (Lluch-Belda *et al.*, 1989; Chavez *et al.*, 2003; Checkley *et al.*, 2017). ELS survival (recruits per egg) and individual egg production (eggs per adult) vary in periodicity on different timescales, and together modulate total sardine recruitment and population abundance over years (Figure 2). While recruitment success follows short-term variations in SST and small prey types during the spring spawning period on a time-scale of 2–4 years, adult individual egg production fluctuates on slightly longer timescales of 3–8 years. The most pronounced sardine abundance fluctuations among our ensemble configurations are driven by a combination of (a) short-term variability in ELS survival determined by SST and ELS food availability, with a smaller contribution of offshore transport, and (b) density-dependent feedbacks in egg production, modulated by local adult food limitation and migration to better feeding habitat under local density limitation.

Together, these processes can produce large sardine peaks at up to 25–34 billion age2+ individuals, which coincides with estimates for the historical sardine peak in 1934 at 27 billion age2+ sardine (Murphy, 1966). These results mirror those of Lindegren *et al.* (2013), who found different timescales of variability in sardine population drivers, for example, recruitment success combined with cohort resonance and long-term climatic forcing to create SPF fluctuations in the CCS. Our mechanistic modelling approach adds detail to this view by resolving dynamic changes in sardine age structure and density-dependence, and demonstrating the relevance of food availability, upwelling strength, and adaptive spatial migration strategies in producing sardine cycles from regional ocean-BGC projections.

Long-term trends under climate change, and sources of uncertainty

The ensemble of model configurations demonstrates that the sardine population is not driven by a single environmental driver in isolation, and provides an estimate for the range of ecological uncertainty in the contributions of environmental drivers and interactions with sardine population processes, as a description of model parameter uncertainty. The overlap in our results with stock assessment, individual-based, and catch distribution (see the "Spatial shift in sardine distribution, and changes in catch distribution among fleets" section) models for the CCS indicates that this ecological uncertainty likely incorporates a considerable part of structural model uncertainty. The ESMs used for our high-resolution, regionally downscaled projections for the CCS were initially selected to

span a range of plausible futures under the IPCC medium and high emission scenarios for the region. They disagree on the rate of surface ocean warming and the direction of changes in primary production, with intermodel variation enveloping the uncertainty among RCP emission scenarios, thus describing the bounds for future environmental parameters (Drenkard *et al.*, 2021; Pozo Buil *et al.*, 2021). In the following, we use specific years in model projections to describe sardine population changes and their causes, while it is important to note that these should not be viewed as predictions for the exact timing of realized changes. The underlying downscaled ESM projections are not designed to reproduce conditions in specific years, but rather to capture long-term trends and exhibit typical fluctuations in environmental parameters.

The warming trend leads to a likely recovery to sardine abundance at or slightly below early 2000s levels by midcentury across ESMs due to increasing recruitment success (Figure 2). Our model ensemble provides some insights into the emergent interactions among temperature and the other drivers from the variation among ESMs, and alternative model configurations with food-dependent processes disabled further illustrate that sardine levels are limited by the variable food availability. Under the GFDL projection, ensemble sardine abundance is limited by food availability for ELS for much of the projection, exacerbated by offshore transport of larvae to areas of lower food. In contrast, faster warming rates in the HAD and IPSL projections override the impacts of ELS and adult food availability in the course of the projections. Density-dependent population feedbacks, together with the divergent trends in different environmental drivers in the downscaled ESM projections, constrain ecological uncertainty in our model after 2060.

The unknown response to temperatures in the future beyond the recorded range represents one of the largest uncertainties for projecting the Pacific sardine population under climate change (Deyle *et al.*, 2013; Checkley *et al.*, 2017). As environmental niches are usually narrowest for spawners and ELS of marine fish (Pörtner and Peck, 2010), we quantify uncertainty in sardine population trends related to ELS thermal windows via sensitivity analysis, accounting for ecological uncertainty across ensemble model configurations.

After 2060, as novel temperature regimes for Pacific sardine ELS emerge, uncertainty related to the thermal window of sardine ELS begins to increase beyond ecological uncertainty (spread of model ensemble configurations) in the fast-warming HAD and IPSL downscaled models, and if T_{opt} is passed, regular sardine stock collapses to below fishable levels occur in the majority of the ensemble configurations after 2070. While sardine abundances at historical peak levels (>40 billion) become more likely under high ocean temperatures after 2060 in the HAD and IPSL projections, the risk of stock collapses to below cut-off limits for sardine fisheries also increases.

These results identify structural uncertainty with regard to ESM input and the biological temperature response as main contributors of uncertainty in long-term projections (2060–2100). The specific year when thermal tolerance uncertainty begins to have a significant effect on the population trajectory varies strongly among model configurations (between 2030 and 2080), depending on the relative contribution of ELS thermal mortality among all environmental drivers.

Earliest impacts of thermal sensitivity on our projections start in the highly temperature-driven model configurations

at a T_{opt} for ELS from 16°C, and latest impacts occur at 17.5°C in the HAD and IPSL projections. This range of T_{opt} with impacts on projections identified from our model calibration period coincides with the results from experimental work: early experiments with Pacific sardine larvae from the CCS found fastest growth rates at 16–17°C (Lasker, 1964), while Japanese sardine (*Sardinops melanostictus*) show optimum growth at 16.2°C (Takasuka *et al.*, 2007) and European sardine (*Sardina pichardus*) experience reduced larval survival at 17°C (Faleiro *et al.*, 2016). Updated physiological experiments with Pacific sardine eggs and larvae from the CCS, possibly under different food conditions, would thus be critical to further constrain the optimum and limit conditions for sardine ELS survival, and reduce long-term uncertainty in our projections.

During periods of less suitable environmental conditions, reductions in sardine landings under the current harvest control rule succeed in dampening impacts and preventing sardine collapses in our model. However, this assumes immediate quota adjustments in the year following a population decrease, with potentially significant socio-economic adaptation costs for sardine fisheries. Furthermore, external impacts on predation and natural mortality (e.g. long-term changes in trophic interactions beyond those during the calibration period) are not yet considered. A scenario-based incorporation of socio-economic and political factors influencing catch and other variables (Hamon *et al.*, 2021), and a detailed analysis of environment-sensitive, multispecies, and other harvest control rules for ameliorating climate change impacts on the sardine stock and fisheries will be undertaken in follow-up work.

Quantifying the linkage to physical parameters and the uncertainty related to BGC parameters will help to advance the realism of long-term projections of marine ecosystems and fish stocks (Payne *et al.*, 2017; Jacox *et al.*, 2020). While ROMS-NEMUCSC achieves a good representation of large-scale distribution patterns for chlorophyll and krill in the CCS (Fiechter *et al.*, 2020, 2021), the skill to reproduce variability in plankton biomass, as in other BGC models, may be lower than for physical variables (Séférian *et al.*, 2020; Kearney *et al.*, 2021). More detailed uncertainty analysis of the BGC model, expanding the ROMS-NEMUCSC hindcast to include the years 2011–20 for further testing and re-calibration of the sardine model, and future updates to the latest generation downscaled CMIP6 runs currently under development, may improve model fit and reduce uncertainty in projections. Our work demonstrates that the combination and timing of changes in multiple physical and lower trophic level variables, not isolated trends in one driver, will determine the fate of SPF stocks under climate change, and should be a focus of further development in ocean and ecological models.

Spatial shift in sardine distribution and changes in catch distribution among fleets

Our model allows adult sardine to adapt to changing ocean conditions by following optimal feeding and spawning locations as they shift through the projection period. This behaviour is consistent with observations of sardine spawning and feeding habitat moving considerably northward after 2014 during a marine heatwave and *El Niño* conditions (Auth *et al.*, 2018; Muhling *et al.*, 2020). Over the course of the model projections, following the optimal SST of 13.5°C,

sardine spawning location moves northward, compressing the stock in the northern half of the CCS after 2060 under the fast-warming HAD and IPSL projections, and after 2080 under GFDL.

Areas of best food availability for sardine move northward at a slower rate than the spawning habitat, to a mean latitude of 39.5° N in the second half of the projection, reducing the northward shift in annual mean sardine distribution. This finding agrees with the results of an individual-based model for Pacific sardine forced with the same downscaled ROMS-NEMUCSC projections, which suggests that the simple migration rules in our model are consistent with the more complex behavioural movement based on prey and temperature cues in the individual-based model (Fiechter *et al.*, 2021).

As fleet availability in our model is responsive to the mean latitudinal position of the sardine stock, catch distribution between the two fleets shows considerable interannual variability, with a more northern sardine stock leading to an increased proportion of catches for the PNW fleet relative to the combined Californian and Mexican fleet, as observed in landing data (Hill *et al.*, 2018). Over the course of the projection, the northward shift in habitat leads to increased availability and a relative increase in catches for the PNW fishing fleet. The projected shift in relative catch between the two fleets matches the trends projected with an individual-based model and a spatial fleet distribution model for Pacific sardine in the CCS, which were driven by the same downscaled ROMS-NEMUCSC projections (Fiechter *et al.*, 2021; Smith *et al.*, 2021).

Besides the projected changes in sardine abundance, the poleward shifts in distribution and catch can be expected to have considerable impacts on sardine fisheries and dependent communities in the CCS, in the second half of the 21st century under the RCP8.5 emissions scenario considered here. However, this analysis is based on the modelled northern subpopulation of Pacific sardine in the CCS. Potentially, reductions projected for the MexCal fisheries could be ameliorated by the southern substock off Baja California, Mexico (which is currently precluded from harvest in US management) migrating increasingly north under continuing warming, and leading to strongest impacts on sardine fisheries at the southern margin of that substock's distribution. Suitable habitat for Pacific sardine in the future may be further constrained by decreases in oxygen availability and increasing acidification in the CCS (Xiu *et al.*, 2018; Howard *et al.*, 2020), which should be treated as additional uncertainties, and warrant further investigation and a precautionary approach for sardine management.

Concluding remarks

We developed a process-based population model that reproduces the last boom and bust of the US Pacific sardine population based on ocean temperature, ELS and adult food, and upwelling strength, and demonstrates that the lack of recovery after 2010 under a warm ocean regime and no fishing can be explained by reduced food availability. The combination and different periodicity of changes in ELS survival and egg production per adult, based on input from downscaled regional ocean models and the population model structure, produce decadal-scale population fluctuations in sardine.

Future projections show a likely recovery of sardine abundance and catch in the middle of the 21st century under the current fisheries management regime, due to increasing

recruitment success under warming ocean temperatures. Long-term trends in the second half of the 21st century are modulated by ELS starvation, density- and food-availability-dependent decreases in egg production per adult, and the adaptive feeding migration of the sardine population. Spatial distribution of Pacific sardine is projected to move to the northern part of the CCS towards the end of the century, with spawning habitat showing a more pronounced shift under ocean warming than the best feeding habitat, which moves north at a slower rate.

On the timescale of 20–50 years into the future, projection uncertainty for Pacific sardine population abundance is determined by ecological uncertainty regarding the contributions of different drivers to population processes, as estimated from our ensemble configurations. Beyond 50–60 years, downscaled ESMs increasingly disagree in the rate of warming, and the physiological temperature optimum for ELS survival becomes the dominant source of uncertainty in the strongly warming HAD and ISPL models. When passing thermal optima, there is considerable risk of sardine stock collapses under all ecological model configurations and ESM projections.

The current harvest control rule buffers temporary sardine stock declines in periods of 2–3 years with unsuitable environmental conditions later in the 21st century. While a variety of socio-economic and political factors will further impact sardine catch in the future, our analysis highlights the value of sustained monitoring of ecosystem conditions and population properties to ensure sustainable fisheries management under continued climate variability and change, for example, to derive environment-responsive harvest control rules (Siple *et al.*, 2019). Underlying process relationships and ecological uncertainty can be constrained further by conducting additional experimental studies and ship-based surveys on Pacific sardine and other fish species.

Our findings open pathways for improving Pacific sardine climate-responsive management under novel environmental conditions in the future, by developing forecasts for recruitment and age class abundance with associated ecological and physiological uncertainties, as some physical ocean variables in the CCS can be forecast with sufficient certainty 1–4 years in advance (Tommasi *et al.*, 2017; Jacox *et al.*, 2020), and sardine adult distribution can be forecast over several months in advance (Kaplan *et al.*, 2016). Advancing population projections informed by biological processes will enable anticipation of emerging phenomena from nonlinear driver interactions, and help distinguish predictable from unpredictable aspects of ecosystem dynamics for marine fish stocks under climate change.

Supplementary data

Author contributions

SK developed and calibrated the model, conducted projections and sensitivity analyses, and drafted the manuscript; MGJ and DT supervised and contributed to development and assessment of the model and projections; MPB and JF contributed physical and plankton hindcasts and projections as model input, and contributed to model development; BAM, PK, and TA provided data and contributed to model development; SB, ELH, and SJB contributed to development and assessment of the model and projections. All authors contributed to writing and revision of the manuscript.

Data availability statement

The data that support the findings of this study are openly available online and in the supplementary material of this article. CalCOFI sardine larvae data are publicly available at https://coastwatch.pfeg.noaa.gov/erddap under dataset ID erdCalCOFIlrvcntQtoSA. Adult age class abundance and catch estimates from the long-term stock assessment model are contained in the supplement of the article.

Conflict of interest statement

The authors declare no competing interests.

References

Auth, T. D., Daly, E. A., Brodeur, R. D., and Fisher, J. L. 2018. Phenological and distributional shifts in ichthyoplankton associated with recent warming in the northeast Pacific Ocean. Global Change Biology, 24: 259–272.

Bakun, A. 2014. Active opportunist species as potential diagnostic markers for comparative tracking of complex marine ecosystem responses to global trends. ICES Journal of Marine Science, 71: 2281–2292.

Bakun, A., Black, B. A., Bograd, S. J., García-Reyes, M., Miller, A. J., Rykaczewski, R. R., and Sydeman, W. J. 2015. Anticipated effects of climate change on coastal upwelling ecosystems. Current Climate Change Reports, 1: 85–93.

Barnes, J. T., MacCall, A. D., Jacobson, L. D., and Wolf, P. 1992. Recent population trends and abundance estimates for the Pacific sardine (*Sardinops sagax*). CalCOFI Reports, 33: 60–75.

Bond, N. A., Cronin, M. F., Freeland, H., and Mantua, N. 2015. Causes and impacts of the 2014 warm anomaly in the NE Pacific. Geophysical Research Letters, 42: 3414–3420.

Brodeur, R. D., Auth, T., and Phillips, A. J. 2019. Major shifts in pelagic micronekton and macrozooplankton community structure in an upwelling ecosystem related to an unprecedented marine heatwave. Frontiers in Marine Science, 6: 212. https://doi.org/10.3389/fmars.2019.00212.

Butler, J. L. 1993. The effect of natural variability of life-history parameters on anchovy and sardine population growth. CalCOFI Reports, 34: 8.

Canales, T. M., Delius, G. W., and Law, R. 2020. Regulation of fish stocks without stock–recruitment relationships: the case of small pelagic fish. Fish and Fisheries, 21: 857–871.

Cavole, L. M., Demko, A. M., Diner, R. E., Giddings, A., Koester, I., Pagniello, C. M. L. S., Paulsen, M.-L. *et al.* 2016. Biological impacts of the 2013–2015 warm-water anomaly in the Northeast Pacific: winners, losers, and the future. Oceanography, 29: 273–285.

Chavez, F. P., Ryan, J., Lluch-Cota, S. E., and C, M. Ñ. 2003. From anchovies to sardines and back: multidecadal change in the Pacific Ocean. Science, 299: 217–221.

Checkley, D. M., Asch, R. G., and Rykaczewski, R. R. 2017. Climate, anchovy, and sardine. Annual Review of Marine Science, 9: 469–493.

Checkley, D. M., and Barth, J. A. 2009. Patterns and processes in the California Current System. Progress in Oceanography, 83: 49–64.

Demer, D. A., Zwolinski, J. P., Byers, K. A., Cutter, G. R., Renfree, J. S., Sessions, T. S., and Macewicz, B. J. 2012. Prediction and confirmation of seasonal migration of Pacific sardine (*Sardinops sagax*) in the California Current Ecosystem. Fishery Bulletin, 110: 52–70.

Deyle, E. R., Fogarty, M., Hsieh, C., Kaufman, L., MacCall, A. D., Munch, S. B., Perretti, C. T. *et al.* 2013. Predicting climate effects on Pacific sardine. Proceedings of the National Academy of Sciences, 110: 6430–6435.

Drenkard, E. J., Stock, C., Ross, A. C., Dixon, K. W., Adcroft, A., Alexander, M., Balaji, V. *et al.* 2021. Next-generation regional ocean projections for living marine resource management in a changing climate. ICES Journal of Marine Science, 78: 1969–1987.

Essington, T. E., Moriarty, P. E., Froehlich, H. E., Hodgson, E. E., Koehn, L. E., Oken, K. L., Siple, M. C. *et al.* 2015. Fishing amplifies forage fish population collapses. Proceedings of the National Academy of Sciences, 112: 6648–6652.

Faleiro, F., Pimentel, M., Pegado, M. R., Bispo, R., Lopes, A. R., Diniz, M. S., and Rosa, R. 2016. Small pelagics in a changing ocean: biological responses of sardine early stages to warming. Conservation Physiology, 4: 1–9.

FAO. 2020. The State of World Fisheries and Aquaculture 2020: Sustainability in Action. Food And Agriculture Organization of the United Nations, Rome, Italy. https://doi.org/10.4060/ca9229en (Last accessed 20 June 2022).

Fiechter, J., Pozo Buil, M., Jacox, M. G., Alexander, M. A., and Rose, K. A. 2021. Projected shifts in 21st century sardine distribution and catch in the California Current. Frontiers in Marine Science, 8: 685241. https://doi.org/10.3389/fmars.2021.685241

Fiechter, J., Santora, J. A., Chavez, F., Northcott, D., and Messié, M. 2020. Krill hotspot formation and phenology in the California Current Ecosystem. Geophysical Research Letters, 47: e2020GL088039. https://doi.org/10.1029/2020GL088039

García-Reyes, M., Sydeman, W. J., Schoeman, D. S., Rykaczewski, R. R., Black, B. A., Smit, A. J., and Bograd, S. J. 2015. Under pressure: climate change, upwelling, and eastern boundary upwelling ecosystems. Frontiers in Marine Science, 2: 19245. https://doi.org/10.3389/fmars.2015.00109

Gómez-Ocampo, E., Gaxiola-Castro, G., Durazo, R., and Beier, E. 2018. Effects of the 2013–2016 warm anomalies on the California Current phytoplankton. Deep Sea Research Part II: Topical Studies in Oceanography, 151: 64–76.

Hamon, K. G., Kreiss, C. M., Pinnegar, J. K., Bartelings, H., Batsleer, J., Catalán, I. A., Damalas, D. *et al.* 2021. Future socio-political scenarios for aquatic resources in Europe: an operationalized framework for marine fisheries projections. Frontiers in Marine Science, 8: 568219. https://doi.org/10.3389/fmars.2021.578516

Hill, K., Crone, P., and Zwolinski, J. 2018. Assessment of the Pacific Sardine Resource in 2018 for U.S. Management in 2018–2019. https://swfsc.noaa.gov/publications/TM/SWFSC/NOAA-TM-NMFS-SWFSC-600.pdf (Last accessed 20 June 2022).

Howard, E. M., Penn, J. L., Frenzel, H., Seibel, B. A., Bianchi, D., Renault, L., Kessouri, F. *et al.* 2020a. Climate-driven aerobic habitat loss in the California Current System. Science Advances, 6: eaay3188. https://doi.org/10.1126/sciadv.aay3188

Jacobson, L. D., and MacCall, A. D. 1995a. Stock-recruitment models for Pacific sardine (*Sardinops sagax*). Canadian Journal of Fisheries and Aquatic Sciences, 52: 566–577.

Jacox, M. G., Alexander, M. A., Siedlecki, S., Chen, K., Kwon, Y.-O., Brodie, S., Ortiz, I. *et al.* 2020. Seasonal-to-interannual prediction

of North American coastal marine ecosystems: forecast methods, mechanisms of predictability, and priority developments. Progress in Oceanography, 183: 102307. https://doi.org/10.1016/j.pocean.2020.102307

Jacox, M. G., Edwards, C. A., Hazen, E. L., and Bograd, S. J. 2018. Coastal upwelling revisited: ekman, bakun, and improved upwelling indices for the U.S. West Coast. Journal of Geophysical Research: Oceans, 123: 7332–7350.

Jacox, M. G., Hazen, E. L., Zaba, K. D., Rudnick, D. L., Edwards, C. A., Moore, A. M., and Bograd, S. J. 2016. Impacts of the 2015–2016 *El Niño* on the California Current System: early assessment and comparison to past events. Geophysical Research Letters, 43: 7072–7080.

Kaplan, I. C., Francis, T. B., Punt, A. E., Koehn, L. E., Curchitser, E., Hurtado-Ferro, F., Johnson, K. F. *et al.* 2018. A multi-model approach to understanding the role of Pacific sardine in the California Current food web. Marine Ecology Progress Series, 617: 1–15. https://doi.org/10.3354/meps12504

Kaplan, I. C., Williams, G. D., Bond, N. A., Hermann, A. J., and Siedlecki, S. A. 2016. Cloudy with a chance of sardines: forecasting sardine distributions using regional climate models. Fisheries Oceanography, 25: 15–27.

Kearney, K. A., Bograd, S. J., Drenkard, E., Gomez, F. A., Haltuch, M., Hermann, A. J., Jacox, M. G. *et al.* 2021. Using global-scale Earth system models for regional fisheries applications. Frontiers in Marine Science, 8: 1121. https://doi.org/10.3389/fmars.2021.622206

Kishi, M. J., Kashiwai, M., Ware, D. M., Megrey, B. A., Eslinger, D. L., Werner, F. E., Noguchi-Aita, M. *et al.* 2007. NEMURO—a lower trophic level model for the north Pacific marine ecosystem. Ecological Modelling, 202: 12–25.

Koenigstein, S., Dahlke, F. T., Stiasny, M. H., Storch, D., Clemmesen, C., and Pörtner, H-O. 2018. Forecasting future recruitment success for Atlantic cod in the warming and acidifying Barents Sea. Global Change Biology, 24: 526–535.

Koenigstein, S., Mark, F. C., Gößling-Reisemann, S., Reuter, H., and Pörtner, H-O. 2016. Modelling climate change impacts on marine fish populations: process-based integration of ocean warming, acidification and other environmental drivers. Fish and Fisheries, 17: 972–1004.

Lasker, R. 1964. An experimental study of the effect of temperature on the incubation time, development, and growth of Pacific sardine embryos and larvae. Copeia, 1964: 399.

Lavaniegos, B. E., and Ohman, M. D. 2007. Coherence of long-term variations of zooplankton in two sectors of the California Current System. Progress in Oceanography, 75: 42–69.

Lindegren, M., and Checkley, D. M. 2013. Temperature dependence of Pacific sardine (*Sardinops sagax*) recruitment in the California Current Ecosystem revisited and revised. Canadian Journal of Fisheries and Aquatic Sciences, 70: 245–252.

Lindegren, M., Checkley, D. M., Rouyer, T., MacCall, A. D., and Stenseth, N. C. 2013. Climate, fishing, and fluctuations of sardine and anchovy in the California Current. Proceedings of the National Academy of Sciences, 110: 13672–13677.

Lluch-Belda, D., Crawford, R. J. M., Kawasaki, T., MacCall, A. D., Parrish, R. H., Schwartzlose, R. A., and Smith, P. E. 1989. World-wide fluctuations of sardine and anchovy stocks: the regime problem. South African Journal of Marine Science, 8: 195–205.

MacCall, A. 1979. Population estimates for the waning years of the Pacific sardine fishery. CalCOFI Reports, 20: 72–82. http://calcofi.org/publications/calcofireports/v20/Vol_20_MacCall.pdf (Last accessed 20 June 2022).

McClatchie, S., Field, J., Thompson, A. R., Gerrodette, T., Lowry, M., Fiedler, P. C., Watson, W. *et al.* 2016. Food limitation of sea lion pups and the decline of forage off central and southern California. Royal Society Open Science, 3: 150628. https://doi.org/10.1098/rsos.150628

McClatchie, S., Goericke, R., Auad, G., and Hill, K. 2010. Re-assessment of the stock–recruit and temperature–recruit relationships for Pacific sardine (*Sardinops sagax*). Canadian Journal of Fisheries and Aquatic Sciences, 67: 1782–1790.

McClatchie, S., Hendy, I. L., Thompson, A. R., and Watson, W. 2017. Collapse and recovery of forage fish populations prior to commercial exploitation. Geophysical Research Letters, 44: 1877–1885. https://doi.org/10.1002/2016GL071751

Muhling, B. A., Brodie, S., Smith, J. A., Tommasi, D., Gaitan, C. F., Hazen, E. L., Jacox, M. G. *et al.* 2020. Predictability of species distributions deteriorates under novel environmental conditions in the California Current System. Frontiers in Marine Science, 7: 589.

Murphy, G. I. 1966. Population biology of the Pacific sardine (*Sardinops caerulea*). Proceedings of the California Academy of Sciences, 4th Series, 34: 1–84.

Neveu, E., Moore, A. M., Edwards, C. A., Fiechter, J., Drake, P., Crawford, W. J., Jacox, M. G. *et al.* 2016. An historical analysis of the California Current circulation using ROMS 4D-Var: system configuration and diagnostics. Ocean Modelling, 99: 133–151.

Nieto, K., McClatchie, S., Weber, E. D., and Cody, C. E. L. 2014. Effect of mesoscale eddies and streamers on sardine spawning habitat and recruitment success off Southern and central California. Journal of Geophysical Research: Oceans, 119: 6330–6339.

NOAA SWFSC. 2022. CalCOFI larvae counts. ERDDAP data server. dataset ID: erdCalCOFIlrvcntQtoSA. https://coastwatch.pfeg.noaa.gov/erddap (Last accessed 20 June 2022).

Payne, M. R., Hobday, A. J., MacKenzie, B. R., Tommasi, D., Dempsey, D. P., Fässler, S. M. M., Haynie, A. C. *et al.* 2017. Lessons from the first generation of marine ecological forecast products. Frontiers in Marine Science, 4. 289. https://doi.org/10.3389/fmars.2017.00289.

Peck, M. A., Alheit, J., Bertrand, A., Catalán, I. A., Garrido, S., Moyano, M., Rykaczewski, R. R. *et al.* 2021. Small pelagic fish in the new millennium: a bottom-up view of global research effort. Progress in Oceanography, 191: 102494. https://doi.org/10.1016/j.pocean.2020.102494

Peck, M. A., Reglero, P., Takahashi, M., and Catalán, I. A. 2013. Life cycle ecophysiology of small pelagic fish and climate-driven changes in populations. Progress in Oceanography, 116: 220–245.

PFMC. 2017. Status of the Pacific Coast Coastal Pelagic Species Fishery and Recommended Acceptable Biological Catches. PACIFIC FISHERY MANAGEMENT COUNCIL, Portland OR. 446pp. www.pcouncil.org/documents/2016/06/stock-assessment-and-fishery-evaluation-2016.pdf (Last accessed 20 June 2022).

Piatt, J. F., Parrish, J. K., Renner, H. M., Schoen, S. K., Jones, T. T., Arimitsu, M. L., Kuletz, K. J. *et al.* 2020. Extreme mortality and reproductive failure of common murres resulting from the northeast Pacific marine heatwave of 2014–2016. PLoS One, 15: e0226087. https://doi.org/10.1371/journal.pone.0226087

Pikitch, E. K., Rountos, K. J., Essington, T. E., Santora, C., Pauly, D., Watson, R., Sumaila, U. R. *et al.* 2014. The global contribution of forage fish to marine fisheries and ecosystems. Fish and Fisheries, 15: 43–64.

Plaganyi, E. E., Punt, A. E., Hillary, R., Morello, E. B., Thebaud, O., Hutton, T., Pillans, R. D. *et al.* 2012. Multispecies fisheries management and conservation: tactical applications using models of intermediate complexity. Fish and Fisheries, 15: 1–22.

Politikos, D. V., Curchitser, E. N., Rose, K. A., Checkley, D. M., and Fiechter, J. 2018. Climate variability and sardine recruitment in the California current: a mechanistic analysis of an ecosystem model. Fisheries Oceanography, 27: 602–622.

Pörtner, H-O., and Peck, M. A. 2010. Climate change effects on fishes and fisheries: towards a cause-and-effect understanding. Journal of Fish Biology, 77: 1745–1779.

Pozo Buil, M., Jacox, M. G., Fiechter, J., Alexander, M. A., Bograd, S. J., Curchitser, E. N., Edwards, C. A. *et al.* 2021. A dynamically downscaled ensemble of future projections for the California Current System. Frontiers in Marine Science, 8: 324. https://doi.org/10.3389/fmars.2021.612874

Punt, A. E., MacCall, A. D., Essington, T. E., Francis, T. B., Hurtado-Ferro, F., Johnson, K. F., Kaplan, I. C. *et al.* 2016. Exploring the

implications of the harvest control rule for Pacific sardine, accounting for predator dynamics: a MICE model. Ecological Modelling, 337: 79–95.

Rijnsdorp, A. D., Peck, M. A., Engelhard, G. H., Mollmann, C., and Pinnegar, J. K. 2009. Resolving the effect of climate change on fish populations. ICES Journal of Marine Science, 66: 1570–1583.

Rykaczewski, R. R., Dunne, J. P., Sydeman, W. J., García-Reyes, M., Black, B. A., and Bograd, S. J. 2015. Poleward displacement of coastal upwelling-favorable winds in the ocean's eastern boundary currents through the 21st century. Geophysical Research Letters, 42: 6424–6431.

Séférian, R., Berthet, S., Yool, A., Palmiéri, J., Bopp, L., Tagliabue, A., Kwiatkowski, L. et al. 2020. Tracking improvement in simulated marine biogeochemistry between CMIP5 and CMIP6. Current Climate Change Reports, 6: 95–119.

Siple, M. C., Essington, T. E., and Plaganyi, E. E. 2019. Forage fish fisheries management requires a tailored approach to balance trade-offs. Fish and Fisheries, 20: 110–124.

Smith, J. A., Muhling, B., Sweeney, J., Tommasi, D., Pozo Buil, M., Fiechter, J., and Jacox, M. G. 2021. The potential impact of a shifting Pacific sardine distribution on U.S. west coast landings. Fisheries Oceanography, 30: 437–454.

Sugihara, G., May, R., Ye, H., Hsieh, C., Deyle, E., Fogarty, M., and Munch, S. 2012. Detecting causality in complex ecosystems. Science, 338: 496–500.

Takasuka, A., Oozeki, Y., and Aoki, I. 2007. Optimal growth temperature hypothesis: why do anchovy flourish and sardine collapse or vice versa under the same ocean regime? Canadian Journal of Fisheries and Aquatic Sciences, 64: 768–776.

Tommasi, D., Stock, C. A, Pegion, K., Vecchi, G. A, Methot, R. D., Alexander, M. A, and Checkley, D. M. 2017. Improved management of small pelagic fisheries through seasonal climate prediction. Ecological Applications, 27: 378–388.

Venrick, E. L. 2012. Phytoplankton in the California Current system off southern California: changes in a changing environment. Progress in Oceanography, 104: 46–58.

Weber, E. D., and McClatchie, S. 2010. Predictive models of northern anchovy Engraulis mordax and Pacific sardine Sardinops sagax spawning habitat in the California Current. Marine Ecology Progress Series, 406: 251–263.

Xiu, P., Chai, F., Curchitser, E. N., and Castruccio, F. S. 2018. Future changes in coastal upwelling ecosystems with global warming: the case of the California Current System. Scientific Reports, 8: 72.

Zwolinski, J. P., and Demer, D. A. 2014. Environmental and parental control of Pacific sardine (Sardinops sagax) recruitment. ICES Journal of Marine Science, 71: 2198–2207.

Zwolinski, J. P., and Demer, D. A. 2019. Re-evaluation of the environmental dependence of Pacific sardine recruitment. Fisheries Research, 216: 120–125.

Zwolinski, J. P., Demer, D. A., Byers, K. A., Cutter, G. R., Renfree, J. S., Sessions, T. S., and Macewicz, B. J. 2012. Distributions and abundances of Pacific sardine (Sardinops sagax) and other pelagic fishes in the California Current Ecosystem during spring 2006, 2008, and 2010, estimated from acoustic–trawl surveys. Fishery Bulletin, 110: 110–122.

Zwolinski, J. P., Emmett, R. L., and Demer, D. A. 2011. Predicting habitat to optimize sampling of Pacific sardine (Sardinops sagax). ICES Journal of Marine Science, 68: 867–879.